EXPLAINING REGIONAL MORTALITY DIFFERENCES WITH AN ECONOMIC-NEURAL MODEL: EVIDENCE FROM EUROPEAN NUTS-2 REGIONS

Donatien Hainaut

LIDAM Discussion Paper ISBA
2026 / 09

UCLouvain

LIDAM
ISBA | Louvain Institute of Data Analysis and Modeling in economics and statistics

ISBA
Voie du Roman Pays 20 - L1.04.01
B-1348 Louvain-la-Neuve
Email : lidam-library@uclouvain.be
https://uclouvain.be/en/research-institutes/lidam/isba/publication

Explaining Regional Mortality Differences with an Economic–Neural Model: Evidence from European NUTS-2 Regions

Donatien Hainaut*
UCLouvain - LIDAM

ABSTRACT This article introduces a novel framework for explaining regional mortality differences across European NUTS-2 areas using macroeconomic indicators. Because regional death rates are substantially noisier than national aggregates, we model age-specific mortality as a smooth B-spline surface whose coefficients are predicted by a feed-forward neural network. The network takes as inputs a set of interpretable regional factors, including GDP per capita, purchasing power, employment rate, educational attainment, and NO2 emissions. Model parameters are estimated via maximization of the Poisson log-likelihood, and the methodology is applied to French regional mortality data. Compared with the Li–Lee multi-population framework, the proposed approach offers several advantages. First, it provides an interpretable link between economic conditions and mortality, allowing the impact of policy-relevant variables to be quantified. Second, the combination of neural networks with B-splines yields smooth, stable mortality curves and avoids the overfitting often observed in non-parametric regional models. Finally, the model is sufficiently robust for long-term mortality forecasting and actuarial applications such as life expectancy projections and annuity valuation.

KEYWORDS : mortality, neural networks, Lee-Carter model, multi-group mortality, life insurance.

1 Introduction

The Lee–Carter (LC) model introduced by Lee and Carter (1992) has served as a cornerstone of mortality forecasting for more than three decades, inspiring a broad family of extensions designed to better capture age, period, and cohort dynamics in population mortality. Subsequent contributions include the cohort-adjusted specification of Renshaw and Haberman (2006), the Cairns–Blake–Dowd class of models (2008), and the extension proposed by Plat (2009). More recent advances rely on functional data representations, such as the transformation-based method of Hyndman et al. (2013), or on machine-learning architectures, as illustrated in Hainaut (2018). Comprehensive overviews of these developments are provided in Booth and Tickle (2011).

Alongside methodological progress, a substantial empirical literature has documented the sensitivity of mortality to macroeconomic conditions. Long-run evidence indicates that improvements

*Corresponding author. Postal address: Voie du Roman Pays 20, 1348 Louvain-la-Neuve Belgium. E-mail to: donatien.hainaut(at)uclouvain.be

in income are associated with lower mortality, as reported by Brenner (2005) for the United States and by Birchenall (2007) for Northwestern Europe. At shorter horizons, however, mortality may exhibit counter-cyclical patterns: Tapia Granados and Roux (2009) show that death rates can fall during recessions, while Ruhm (2005) discusses econometric challenges underlying such findings. These observations have motivated models that incorporate economic drivers directly into the mortality structure. French and O'Hare (2014) demonstrated that adding exogenous covariates improves the predictive accuracy of the LC framework; Boonen and Li (2017) extended the Li–Lee coherent model (Li and Lee, 2005) by embedding GDP information; Dimai (2024) expanded the set of explanatory factors to include economic, environmental, and lifestyle variables for a large panel of countries; and Villegas et al. (2025) examined socio-economic heterogeneity using cause-of-death modeling. A related multi-population extension relying on economic and environmental time series is presented in Hainaut (2026).

Despite these contributions, relatively little work has focused on mortality modelling at the regional level. In Europe, NUTS-2 regions represent key statistical units, yet their comparatively small populations generate substantially noisier mortality rates than national aggregates. This poses challenges for models relying on non-parametric structures, such as the Li–Lee framework, which tend to overfit when applied to smaller populations. Moreover, regional mortality outcomes are shaped by socio-economic and environmental disparities that are not fully captured by approaches relying only on demographic latent factors.

To address these issues, this article develops a modelling framework in which regional mortality is represented through a smooth B-spline surface whose coefficients are predicted by a feed-forward neural network. The network uses interpretable regional covariates, GDP per capita, purchasing power, employment rate, educational attainment, and NO_2 emissions, to explain heterogeneity across regions. The use of B-splines ensures stable and smooth age profiles, while the neural component allows the model to embed nonlinear interactions between economic conditions, region-specific characteristics, and calendar time. Compared with earlier approaches relying either on purely demographic structures or on principal-component reductions of external variables (e.g., Niu and Melenberg 2014; Boonen and Li 2017), the proposed model directly incorporates a richer set of explanatory factors and mitigates overfitting through its constrained spline representation.

The remainder of the article is organized as follows. Section 2 presents the neural-spline model and describes the economic covariates used as inputs. Section 3 details the SVD-based approach used to forecast regional economic variables and generate prospective mortality tables. Section 4 compares the proposed model with the LC and Li–Lee benchmarks using French and Belgian regional data. Section 5 concludes.

2 Model

We rely on mortality and economic data for European NUTS-2 regions sourced from the Eurostat database[1]. These statistics can be accessed through the Eurostat API, which facilitates automated extraction and preprocessing directly in Python. For each country, let $D_{x,t,g}$ denote the recorded number of deaths at age x, during calendar year t, in region g. The age range varies across countries but typically covers ages from 0 up to a maximum between 80 and 85; we denote the lower and upper bounds by x_m and x_M. The available time horizon also differs by country, as it is constrained by the coverage of the associated economic and environmental indicators. In the empirical work presented here, the French dataset spans 2000–2023, while the

[1]https://ec.europa.eu/eurostat/web/main/data/database

Belgian dataset covers 2000–2024.

Because NUTS-2 regions often have relatively small populations, crude death rates computed directly from observed counts can be highly volatile. To mitigate this issue, we adopt a parametric framework that combines a feed-forward neural network with a B-spline representation of age-specific mortality. Let t_m and t_M denote the first and last calendar years available, and let n_g be the number of NUTS-2 regions in the country under study. Eurostat also reports exposures $E_{x,t,g}$ and crude death rates $\mu_{x,t,g}$ for each age-region-year combination.

Following Brouhns et al. (2002), we assume that the number of deaths, $D_{x,t,g}$ follows a Poisson law with mean equal to exposure multiplied by the force of mortality:

$$D_{x,t,g} \quad \sim \quad Po\left(E_{x,t,g}\mu_{x,t,g}\right) .$$

This specification yields a likelihood function that is equivalent to a binomial formulation but offers improved numerical stability. The probability of observing $d_{x,t,g}$ deaths is therefore

$$P\left(D_{x,t,g} = d_{x,t,g}\right) \quad = \quad \frac{\exp\left(-\mu_{x,t,g}\, E_{x,t,g}\right)\left(\mu_{x,t,g}\, E_{x,t,g}\right)^{d_{x,t,g}}}{d_{x,t,g}!} .$$

Factors	**Dataset names**	**Variables**
Mortality	demo_r_mlife	DEATHRATE
		PYLIVED
		NUMBERDYING
GDP	nama_10r_2gdp	EUR_HAB_EU27_2020
Households	nama_10r_2hhinc	PPS_EU27_2020_HAB
Education	edat_lfse_04	ED0-2 , T, Y25-64
		ED3_4 , T, Y25-64
		ED5-8 , T, Y25-64
Employment	lfst_r_lfe2emprt	T, Y25-64
NO2	EDGAR_2025_GHG_NUTS2	N2O

Table 1: List of datasets and variables used by the NN model. Except NO2 data coming from EDGAR, all other statistics come from Eurostat.

We link regional mortality patterns to a collection of explanatory variables listed in Table 1. The first covariate is regional GDP per capita, expressed relative to the EU27 (2020) benchmark; this variable is denoted by $u_{t,g}^{(gdp)}$ for all years $t \in [t_m, t_M]$ and for each region $g = 1$ to n_g. The second indicator, $u_{t,g}^{(pps)}$, represents the Purchasing Power Standard (PPS) per inhabitant, likewise measured as a percentage of the EU27 (2020) average. A third economic variable, $u_{t,g}^{(emp)}$, captures labour-market conditions and corresponds to the employment rate among individuals aged 25–64 in region g during year t.

We further include a factor capturing differences in regional educational attainment. For this purpose, we use the percentage of individuals aged 25–64 with

- Lower secondary, upper secondary and post-secondary non-tertiary education (ED34),
- Tertiary education (ED58).

From these two measures, we construct a composite index intended to approximate the average duration of post-secondary studies. This index is defined as

$$u_{t,g}^{(edu)} = (ED34_{t,g} \times 4 + ED58_{t,g} \times 8)/100 .$$

The final environmental factor is the regional emission of NO2, expressed in kilotonnes of CO2 equivalent per square kilometer. We denote this variable by $u_{t,g}^{(no_2)}$. Annual emission volumes are obtained from the Emissions Database for Global Atmospheric Research (EDGAR)[2]. NO2 emissions result primarily from the combustion of fossil fuels, and elevated concentrations are known to cause respiratory irritation and related symptoms such as coughing and shortness of breath. The surface area of each NUTS-2 region (in square kilometers) is computed using the Python library **geopandas**, allowing us to express emissions on a per-area basis.

In what follows, we denote the vector of economic factors by

$$\boldsymbol{u}_{t,g} = \left(u_{t,g}^{(gdp)}, u_{t,g}^{(pps)}, u_{t,g}^{(emp)}, u_{t,g}^{(edu)}, u_{t,g}^{(no_2)}\right)^\top .$$

We assume that log-mortality rates depend on these variables, as well as on the region and the calendar year, through a nonlinear function represented as a linear combination of B-splines. To construct this basis, we divide the interval between x_m and x_M into m equidistant sub-intervals and denote by d the degree of the B-splines. This construction yields $m+1$ knots. Setting $\Delta_m := \frac{x_M - x_m}{m}$, the knots are defined for $j = 0$ up to $m + 2d$ by

$$x_j = x_m - (d - j)\,\Delta_m .$$

We denote by $B_{j,d}(x)$, the B-spline or order d associated with the j^{th} knot. Let us recall that B splines are defined recursively:

$$B_{j,0}(x) = \begin{cases} 1 & x_j \leq x < x_{j+1} \\ 0 & \text{otherwise} , \end{cases}$$

and

$$B_{j,n}(x) \quad = \quad \frac{x - x_j}{x_{j+n} - x_j} B_{j,n-1}(x) + \frac{x_{j+n+1} - x}{x_{j+n+1} - x_{j+1}} B_{j+1,n-1}(x) .$$

Using B-splines rather than alternative interpolation schemes offers several advantages: the basis functions have compact support, rely on low-degree piecewise polynomials, and combine smoothly, which avoids oscillatory behaviour and improves numerical stability.

We assume that log-mortality rates can be written as

$$\ln\left(\mu_{x,t,g}\right) \quad = \quad \sum_{j=0}^{m+d-1} w_j\left(t, g, \boldsymbol{u}_{t,g} | \Omega\right) B_{j,d}(x) ,$$

where $\boldsymbol{w} = \left(w_j\left(t, g, \boldsymbol{u}_{t,g} | \Omega\right)\right)_{j=0,\dots,m+d-1}$ is the output vector of a feed-forward neural network, $\boldsymbol{w} = F\left(t, E\left(g\right), \boldsymbol{u}_{t,g} | \Omega\right)$ parametrized by a set of neural weights, Ω. The network takes as input an embedding $E\left(g\right)$ of the region index g, represented as a numerical vector of dimension n_e. We now briefly recall the definitions of the feed-forward architecture and the embedding layer.

Definition Let $n_e \in \mathbb{N}$ be the dimension of the embedding vector and n_g the number of levels of g. We denote by $\boldsymbol{e}_g \in \{0,1\}^{n_g}$ the one-hot encoding vector of g. Let $W \in \mathbb{R}^{n_g \times n_e}$. The embedding layer is a function $E : \{1, ..., n_g\} \to \mathbb{R}^{n_e}$ defined by

$$E\left(g\right) = \boldsymbol{e}_g^\top W .$$

Definition Let l, n_0, n_1, ..., $n_l \in \mathbb{N}$ be respectively the number of layers and neurons in each

[2] edgar.jrc.ec.europa.eu/dataset_ghg2025_nuts2

layer. n_0 is also the size of input vector. The activation function of layer $k = 1, 2, ..., l$ is noted $h_k(.) : \mathbb{R} \to \mathbb{R}$. Let $C_k \in \mathbb{R}^{n_k} \times \mathbb{R}^{n_{k-1}}$ and $\boldsymbol{c}_k \in \mathbb{R}^{n_k}$ for $k = 1, ..., l$, be neural weights defining the input, intermediate and output layers. We define the following functions

$$\psi_k(\boldsymbol{v}) = h_k \left(C_k \boldsymbol{v} + \boldsymbol{c}_k \right), k = 1, ..., l$$

where the activation functions $h_k(.)$ are applied component wise. The neural network is a function $F_\Omega : \mathbb{R}^{n_0} \to \mathbb{R}^{n_l}$ defined by

$$F(\boldsymbol{v}|\Omega) \quad = \quad \psi_l \circ \psi_{l-1} \circ ... \circ \psi_1(\boldsymbol{v}) .$$

In our framework, the input vector of the neural network is $\boldsymbol{v}_{t,g} = (t, E(g), \boldsymbol{u}_{t,g})$, of dimension $6 + n_e$, while the output dimension is $m + d - 1$. Figure 1 illustrates the architecture used in the numerical application: an embedding layer of dimension $n_e = 4$, followed by a feed-forward network of sizes $l = 4$, $n_0 = 10$, $n_1 = 20$, $n_2 = 16$, $n_3 = 8$ and $n_4 = 4$. The final layer serves as a bottleneck, limiting model complexity and reducing the risk of overfitting the regional death rates. In the empirical analysis, we employ B-splines of degree d =3 with the number of knots m ranging from 10 to 20.

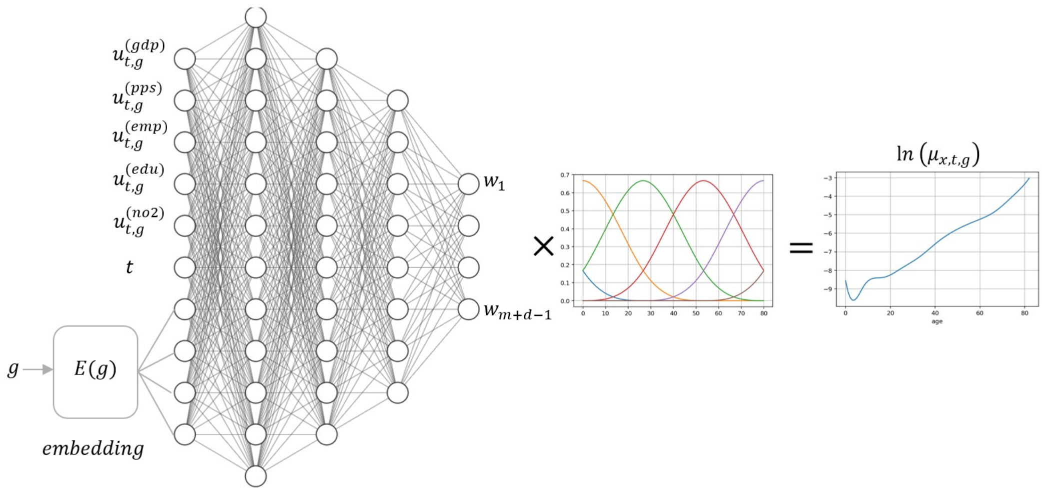

Figure 1: Workflow of the model

The vector Ω of neural weights is estimated by maximizing the Poisson log-likelihood,

$$\hat{\Omega} \quad = \quad \arg\max_{\Omega} \ln \mathcal{L}(\Omega) ,$$

where the log-likelihood is computed over all ages, calendar years, and regions:

$$\mathcal{L}(\Omega) = \sum_{x=x_m}^{x_M} \sum_{t=t_m}^{t_M} \sum_{g=1}^{n_g} \ln \left(\frac{\exp(-\mu_{x,t,g} E_{x,t,g}) (\mu_{x,t,g} E_{x,t,g})^{d_{x,t,g}}}{d_{x,t,g}!} \right) \tag{1}$$

Expanding the logarithm yields

$$\mathcal{L}(\Omega) = \sum_{x=x_m}^{x_M} \sum_{t=t_m}^{t_M} \sum_{g=1}^{n_g} \left(d_{x,t,g} \ln(\mu_{x,t,g}) - \mu_{x,t,g} E_{x,t,g} + d_{x,t,g} \ln(E_{x,t,g}) - \log(d_{x,t,g}!) \right)$$

Up to an additive constant, this expression is proportional to

$$\mathcal{L}(\Omega) \propto \sum_{x=x_m}^{x_M} \sum_{t=t_m}^{t_M} \sum_{g=1}^{n_g} \left(d_{x,t,g} \ln(\mu_{x,t,g}) - E_{x,t,g} \exp(\ln(\mu_{x,t,g})) \right) .$$

Letting $\hat{d}_{x,t,g} = E_{x,t,g}\mu_{x,t,g}$, enote the expected number of deaths implied by the model, the log-likelihood can therefore be written, up to proportionality, as

$$\mathcal{L}(\Omega) \;\propto\; \sum_{x=x_m}^{x_M}\sum_{t=t_m}^{t_M}\sum_{g=1}^{n_g}\left(d_{x,t,g}\ln\left(\mu_{x,t,g}\right) - \hat{d}_{x,t,g}\right).$$

The neural network is implemented in TensorFlow (Python), and the log-likelihood is maximized via gradient descent. The learning rate is fixed at 10^{-4}, and training is stopped when the log-likelihood fails to improve by more than 0.01 over the last 100 iterations.

3 Mortality forecasting

Actuarial applications require a model capable of producing reliable long-term forecasts of mortality rates. For instance, valuing a life annuity purchased at age 60 in 2026 requires prospective mortality tables extending to at least 2076, assuming an ultimate age of 110. Because our model links mortality to regional economic conditions, long-horizon mortality projections necessitate forecasting these economic variables as well. One could, in principle, build a dedicated neural architecture for this purpose, such as a recurrent network with long–short term memory (LSTM) layers, as discussed in Chapter 8 of Denuit et al. (2019), to capture temporal dependencies in regional indicators. However, such models require long historical time series to be reliably trained. In practice, fewer than 30 annual observations are available for most regional economic variables, making complex sequence-based machine-learning approaches unsuitable.

For this reason, we adopt a more robust and parsimonious alternative based on a singular value decomposition (SVD) of the data matrix. In a first step, the dimensionality of the economic dataset is reduced to a small number of principal factors that capture the dominant temporal and regional patterns. These factors are then extrapolated using a multivariate random walk. Despite its simplicity, this approach proves adequate because the observed trajectories of regional economic variables typically follow relatively smooth, noisy linear trends. The SVD-based reduction filters out high-frequency noise and allows the extrapolation to focus on the stable long-term components that drive mortality forecasts.

We denote by n_y, the number of years of observations and by n_g the number of regions. The yearly economic variables are stored in an $(n_y \times 5n_g)$-matrix M. The t^{th} row of M is the vector $\boldsymbol{m}_t = (\boldsymbol{u}_{t,1}, \ldots, \boldsymbol{u}_{t,g})$ which concatenates the five economic factors for all regions in year t. We factorize this matrix using a singular value decomposition (SVD),

$$M = U\,\Lambda\,V^{\top}.$$

where U is a $n_y \times n_y$ unitary matrix, Λ is an $(n_y \times 5n_g)$ rectangular diagonal matrix with non-negative singular values on the diagonal and V is a $(5n_g \times 5n_g)$ unitary matrix V. The singular values in Λ are ordered from largest to smallest.

We approximate M using only the n_z largest singular values. Let U_{n_z} and V_{n_z} denote the first n_z columns of U and V and Let Λ_{n_z} be the top-left $n_z \times n_z$ block of Λ. The resulting rank-n_z approximation of M is:

$$\hat{M} = U_{n_z}\,\Lambda_{n_z}\,V_{n_z}^{\top}.$$

The reduced representation of data is the $(n_y \times n_z)$-matrix:

$$Z \;=\; U_{n_z}\,\Lambda_{n_z}.$$

The j^{th} column of Z provides the time-series of the j^{th} principal factor, and its rows define the multivariate sequence

$$\boldsymbol{z}_t = (z_{t,1}, ..., z_{t,n_z}) \ , \ t = 1, ..., n_y .$$

We extrapolate these factors using a multivariate random walk,

$$\boldsymbol{z}_{t+1} \quad = \quad \boldsymbol{z}_t + \boldsymbol{\epsilon}_t \, , \quad \forall t \geq t_M ,$$

where $\boldsymbol{\epsilon}_t \sim \mathcal{N}(\boldsymbol{\mu_z} \, , \Sigma_z)$. $\boldsymbol{\mu_z}$ and Σ_z, are the sample mean vector and empirical covariance matrix computed from $(\boldsymbol{z}_t)_{t=t_m,...,t_M}$. For each simulated trajectory $\left(\boldsymbol{z}_{t+1}^{(i)}\right)_{i=1,...n_{sim}}$, we forecast vectors of economic variables at time $t+1$ as follows:

$$\boldsymbol{m}_{t+1}^{(i)} \quad = \quad \boldsymbol{z}_{t+1}^{(i)} V_{n_z}^{\top} + \boldsymbol{\Delta_m} \, , \forall t \geq t_M \, , \, i = 1, ..., n_{sim}$$

where $\boldsymbol{\Delta_m} = \boldsymbol{m}_{t_M} - \hat{\boldsymbol{m}}_{t_M}$ is a vector of adjustment terms ensuring that forecasts remain aligned with the most recently observed economic conditions. Each forecasted vector, $\boldsymbol{m}_{t+1}^{(i)} = \left(\boldsymbol{u}_{t+1,1}^{(i)}, \ldots, \boldsymbol{u}_{t+1,g}^{(i)}\right)$, provides, for each region g, a projected set of economic covariates that serve as inputs to the neural network. In the i^{th} simulation, age-specific death rates are then computed using the B-spline representation of mortality:

$$\mu_{x,t+1,g}^{(i)} \quad = \quad \exp\left(\sum_{j=0}^{m+d-1} w_j\left(t+1, g, \boldsymbol{u}_{t+1,g}^{(i)} \,|\, \Omega\right) B_{j,d}(x)\right) \, , \, i = 1, ..., n_{sim} \, .$$

4 Numerical illustration

We test the NN model on regional mortality data for continental France (FR) and Belgium (BE). Although the two countries are geographically contiguous, they exhibit markedly different economic structures, growth patterns, and regional socio-economic disparities. These contrasts justify treating their mortality dynamics as distinct systems. FR and BE respectively comprise 22 and 11 NUTS2 regions. Due to data availability in Eurostat, the French analysis uses a time window from 2000 to 2023 for France and 2024 for Belgium.

We focus on the mortality of the overall population and do not distinguish by gender for two main reasons. First, developing separate forecasting models for male and female death rates would double the number of sub-populations and lead to noisier crude mortality rates due to smaller sample sizes. Second, EU regulations prohibit the use of gender-based mortality tables in actuarial applications, making gender-specific modelling unsuitable for our purposes. Mortality data cover ages 0 to 85, but we restrict attention to ages 0 to 82, as death rates above this threshold become increasingly noisy because of the small regional population sizes at advanced ages.

As benchmark, we consider the Lee-Carter model and a variant of the Li-Lee model. In this article, the Lee–Carter model (LC) is estimated on regional data, assuming the following dynamic for log-mortality rates:

$$\ln\left(\mu_{x,t,g}^{LC}\right) = \alpha_x^{LC} + \beta_x^{LC} \kappa_t^{LC} \, .$$

The α_x, β_x and κ_t are estimated by maximization of the sum of Poisson log-likelihoods across regions. This model is non-parametric and therefore involves $2(x_M - x_m) + (t_M - t_m)$ degrees of freedom. To ensure identifiability, the parameters are scaled such that:

$$\sum_{t=t_m}^{t_M} k_t^{LC} = 0 \quad , \quad \sum_{x=x_m}^{x_M} \beta_x^{LC} = 1 \, . \tag{2}$$

The second benchmark is a variant of the Li and Lee (LL) model. In this multi-population framework, the force of mortality is modeled as:

$$\ln\left(\mu_{x,t,g}^{LL}\right) = \alpha_x^{LL} + \beta_x^{LL}\kappa_t^{LL} + \beta_{x,g}^{LL}\kappa_{g,t}^{LL} .$$

As in the LC model, parameters are estimated by iterative maximization of the Poisson log-likelihood, with identifiability constraints applied to ensure proper scaling. Since this model is non-parametric, the number of degrees of freedom is large: $(g_M+2)\,(x_M-x_m)+(g_M+1)\,(t_M-t_m)$. Because the population size in NUTS2 regions is relatively small compared to national populations, this model tends to overfit the data and produces irregular mortality curves as illustrated in a following subsection.

4.1 Goodness of fit

We estimate a range of neural network specifications combining B-splines with different levels of flexibility. The number of knots m is set to 10, 15, and 20, B-splines of degrees d=3 and 4 are considered, and the feed-forward network includes three hidden layers. Rectified Linear Units (ReLU), $h(v) = \max(0, v)$, are used as activation functions in the hidden layers, while the output layer is linear. Tables 2 and 3 summarize the corresponding goodness-of-fit statistics for France and Belgium.

Relative to the Lee–Carter (LC) model, all neural network specifications yield a substantial improvement in log-likelihood, reflecting their enhanced ability to capture regional mortality heterogeneity. Although neural networks involve a larger number of parameters than the Li–Lee (LL) model, they do not exhibit the same degree of overfitting. This is because the network predicts the coefficients of a B-spline representation rather than reconstructing age-specific mortality rates directly. As a result, the log-likelihood values obtained with the neural network are generally comparable to, or slightly lower than, those of the LL model, despite the latter's much higher flexibility.

For France, the highest log-likelihood is achieved by the (64,32,16) network with 20 knots and B-splines of degree four. This specification attains a fit close to the LL model in terms of likelihood. However, both the Akaike and Bayesian Information Criteria (AIC and BIC) penalize the neural network more heavily than the LL model due to its larger parameter count. Based on the AIC, the (32,16,8) network with 20 knots and B-splines of degree four offers the best trade-off between goodness of fit and complexity. It also outperforms the LL model. Subsequent analyses will be based on this architecture.

n_1	n_2	n_3	m	d	**dofs**	$\ln \mathcal{L}(\Omega)$	**AIC**	**BIC**	**Time**	**epoch**
32	16	8	10	3	1221	-152251.92	306945.84	317553.81	21.54	16363
32	16	8	15	3	1266	-149208.5	300949.01	311947.94	23.06	17823
32	16	8	20	3	1311	-148686.7	299995.41	311385.29	18.35	14423
32	16	8	10	4	1230	-152460.6	307381.21	318067.37	26.41	19999
32	16	8	15	4	1275	-149919.47	302388.94	313466.06	24.73	19999
32	16	8	20	4	1320	-148010.63	298661.26	310129.34	25.39	19999
64	32	16	10	3	3621	-151994.73	311231.47	342690.49	18.29	12991
64	32	16	15	3	3706	-148028.67	303469.34	335666.84	17.64	12667
64	32	16	20	3	3791	-147525.44	302632.88	335568.85	19.81	14861
128	64	32	10	4	12294	-150461.57	325511.15	432320.64	30.69	19999
128	64	32	15	4	12459	-147510.57	319939.14	428182.14	31.47	19999
128	64	32	20	4	12624	-148180.5	321609.0	431285.52	25.36	13332
64	32	16	10	4	3638	-149903.59	307083.18	338689.9	25.68	19999
64	32	16	15	4	3723	-147277.42	302000.83	334346.02	31.84	19999
64	32	16	20	4	3808	-147102.5	301821.0	334904.66	26.73	16381
			NA	NA	190	-195194.81	390769.62	392420.33		
			NA	NA	2544	-145907.37	296902.73	319004.84		

Table 2: Statistics of goodness of fit, France. dofs: number of degrees of freedom. AIC and BIC: Akaike and Bayesian information criteria.

n_1	n_2	n_3	m	d	**dofs**	$\ln \mathcal{L}(\Omega)$	**AIC**	**BIC**	**Time**	**epoch**
32	16	8	10	3	1177	-65444.92	133243.83	142701.75	16.22	13491
32	16	8	15	3	1222	-64939.31	132322.63	142142.15	18.92	14718
32	16	8	20	3	1267	-64952.18	132438.35	142619.47	20.51	15704
32	16	8	10	4	1186	-65429.83	133231.65	142761.89	26.98	19999
32	16	8	15	4	1231	-65001.16	132464.33	142356.17	23.15	19999
32	16	8	20	4	1276	-64945.88	132443.76	142697.2	22.72	19265
64	32	16	10	3	3577	-65461.58	138077.17	166820.55	14.07	10830
64	32	16	15	3	3662	-64726.93	136777.87	166204.28	16.26	12693
64	32	16	20	3	3747	-64658.96	136811.93	166921.37	18.55	14270
64	32	16	10	4	3594	-64987.54	137163.08	166043.07	25.01	19999
64	32	16	15	4	3679	-64577.14	136512.29	166075.3	23.28	17525
64	32	16	20	4	3764	-64590.19	136708.39	166954.43	19.58	14369
128	64	32	10	3	12217	-65544.55	155523.09	253694.16	13.53	9201
128	64	32	15	3	12382	-64840.41	154444.81	253941.76	14.38	9704
128	64	32	20	3	12547	-64805.28	154704.55	255527.37	14.16	8467
			NA	NA	191	-81491.91	163365.81	164900.61		
			NA	NA	1379	-64343.05	131444.1	142525.21		

Table 3: Statistics of goodness of fit, Belgium. dofs: number of degrees of freedom. AIC and BIC: Akaike and Bayesian information criteria.

For Belgium, the best-performing specification, according to the AIC, is the (32,16,8) network, this time with 15 knots and B-splines of third degree. Its AIC is close to the one of the LL model. We will investigate the properties of this model in the next paragraphs. As in the French case, neural networks with more neurons are strongly penalized by the AIC and BIC.

Table 4 and 5 in Appendix A, report exposure-weighted mean absolute errors between observed and predicted death rates. For each region $g = 1, ..., G$, The weighted mean absolute errors (WMAE) is defined as:

$$WMAE_g = \frac{1}{\sum_{x,t} E_{x,t,g}} \sum_{x,t} E_{x,t,g} \left| \mu_{x,t,g} - \hat{\mu}_{x,t,g} \right| ,$$

where $E_{x,t,g}$ denotes the exposure and $\mu_{x,t,g}$, $\hat{\mu}_{x,t,g}$ are the observed and fitted death rates, respectively.

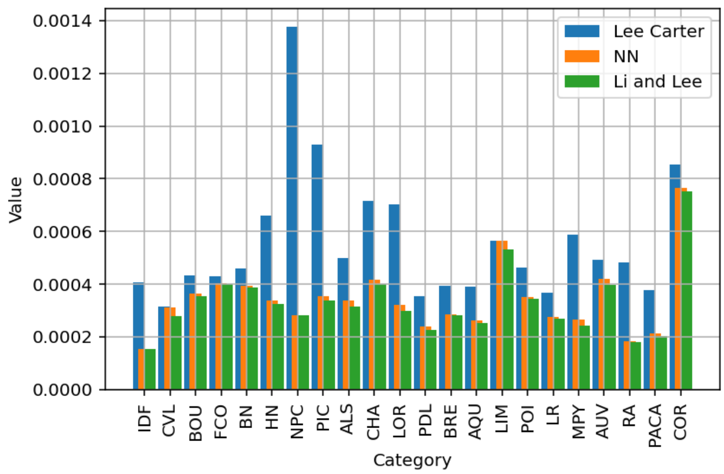

Figure 2: Histogram of weighted mean absolute errors by regions, France.

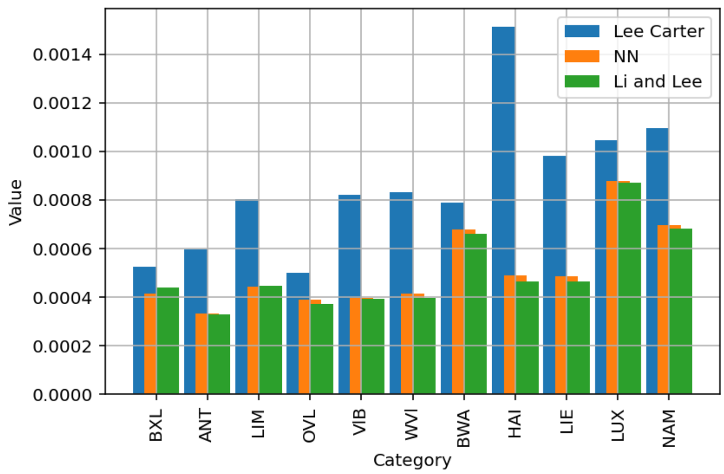

Figure 3: Histogram of weighted mean absolute errors by regions, Belgium.

Figure 2 compares the regional WMAEs for French regions obtained with the neural network model (32,16,8, m=20,d=4), the Lee–Carter (LC) model, and the Li–Lee (LL) model. Figure 3 provides the corresponding comparison for Belgium using the (32,16,8, m=15, d=3) neural network.

These histograms highlight the strong ability of the neural network model to capture regional mortality heterogeneity through economic covariates. The regional prediction errors are generally of the same order of magnitude as those obtained with the LL model, while remaining substantially lower than those of the LC model in many regions. In France, the neural network markedly improves upon the LC fit in several regions, including Nord–Pas-de-Calais (−79.46% WMAE), Picardie (−61.99%), and Lorraine (−54.25%). In contrast, the reduction in error is more limited in Limousin and Corse, where mortality rates exhibit high volatility due to small population sizes. Corse (approximately 360 000 inhabitants) and Limousin (around 710 000 inhabitants) are among the least populous French regions, which amplifies measurement noise in crude death rates.

Similar patterns are observed in Belgium. The largest error reductions relative to the LC model are found in Hainaut (−67.60%) and Vlaams Brabant (−51.58%). Conversely, modeling errors remain comparatively high in Luxembourg, Brabant Wallon, and Namur (with populations of approximately 415 000, 415 381, and 505 000 inhabitants, respectively). As in the French case, the limited population size in these regions is the primary source of increased measurement error in observed mortality rates.

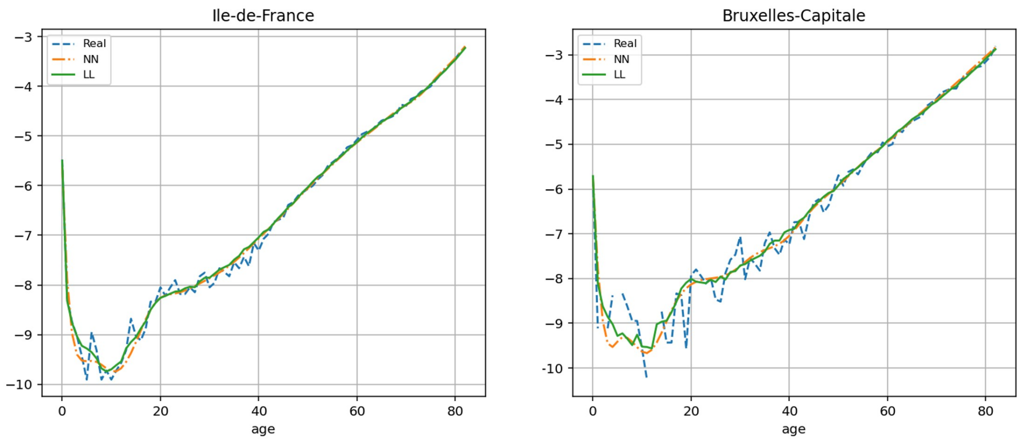

Figure 4: Comparison of NN, LL and observed log-mortality rates for the year 2016, Ile-de-France.

Figure 4 presents the modeled and observed log-mortality rates for Ile-de-France and Bruxelles-Capitale in 2016. By construction, the neural network model produces smooth age-specific mortality curves across the entire lifespan, a property that is particularly desirable for actuarial applications such as life insurance and annuity pricing. In contrast, the Li–Lee (LL) model generates noticeably more irregular mortality profiles. Although the LL model attains a high in-sample goodness of fit, its fully non-parametric structure leads to overfitting of age-specific noise, resulting in erratic mortality patterns that are less suitable for extrapolation and pricing purposes.

Figures 5 and 6 display the spatial distribution of weighted mean absolute errors (WMAEs) for the Lee–Carter (LC) and neural network (NN) models across France and Belgium. In France, the error maps indicate that the NN model does not favor any particular geographical area, but instead delivers a balanced and globally consistent fit across regions. No systematic spatial pattern in the WMAEs emerges, and the largest errors are concentrated in less populous regions, where mortality rates are inherently more volatile.

The Belgian maps confirm a widespread reduction in errors relative to the LC model. As in the French case, the regions exhibiting the largest NN errors are located in the southern part of Belgium and correspond to the least populous areas. This spatial distribution reinforces the conclusion that remaining discrepancies are primarily driven by data sparsity rather than by structural misspecification of the model.

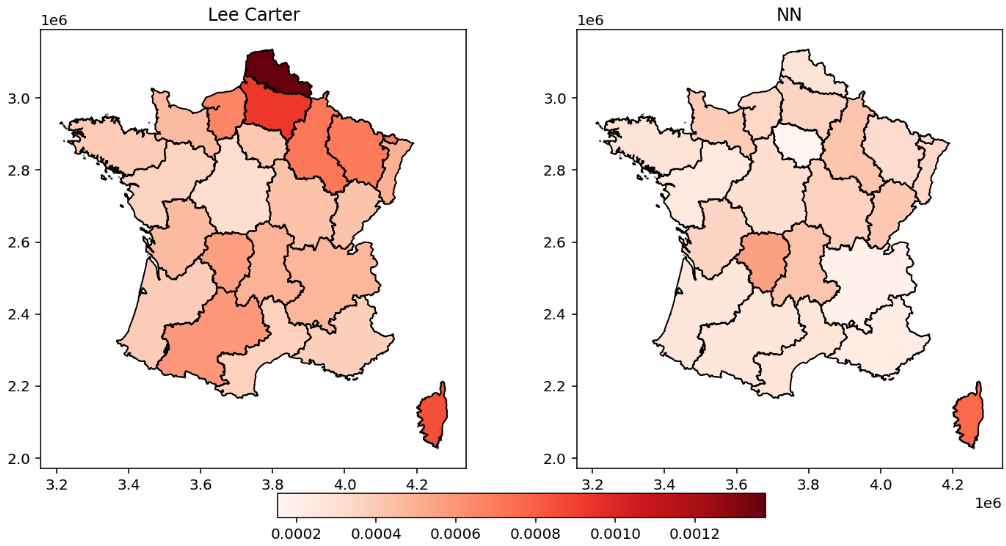

Figure 5: Left and right plots: maps of WMAEs with the Lee-Carter and the NN models. France.

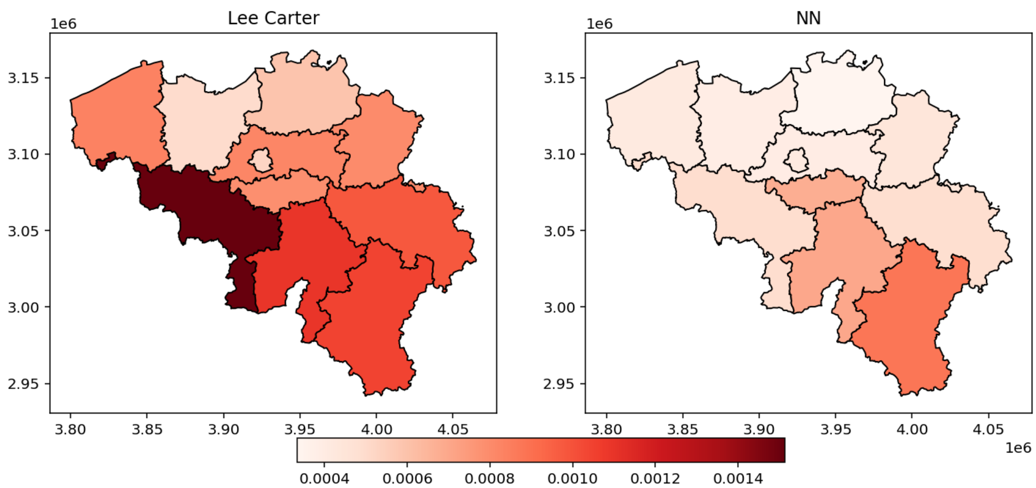

Figure 6: Left and right plots: maps of WMAEs with the Lee-Carter and the NN models. Belgium.

4.2 Evolution of life expectancy

To assess the impact of economic conditions on longevity, we jointly forecast mortality and economic conditions over a ten-year horizon. Economic variables are extrapolated using the SVD-based procedure described in Section 3, retaining the first $n_z = 2$ principal factors. Higher-order components are excluded, as they do not exhibit clear long-term trends. We generate 1000 stochastic trajectories for these factors. As illustrated in Figure 7 for France, the two retained components display stable linear trends over the period 2000–2023, punctuated by two marked shocks corresponding to the 2008 financial crisis and the 2020 COVID-19 pandemic. The second factor is noticeably more volatile during the pandemic period. The orange curves represent the average projected paths generated by the random-walk extrapolation. Results for Belgium are not displayed, as the principal factors exhibit very similar dynamics.

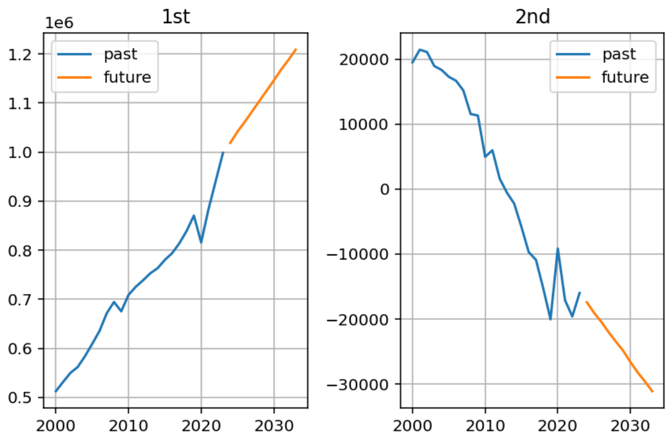

Figure 7: Principal factors and their average extrapolated values, France.

Tables 6 and 7 in Appendix B summarize the average regional growth rates of the simulated economic variables. In France, the lowest and highest projected GDP growth rates are respectively observed in Champagne (1.29 %) and Corse (1.85 %). Average purchasing power growth peaks at approximately 1.44 % in Bretagne, Basse-Normandie, Rhône-Alpes, and PACA, while Picardie records the lowest increase (1.31 %). The strongest improvements in the educational index are forecast in Nord-Pas-de-Calais (1.75 %) and Corse (2.27 %). Employment growth ranges from 0.89 % in Picardie to 1.60 % in Corse. Finally, NO2 emissions exhibit heterogeneous dynamics, decreasing by up to −1.16 % in Haute-Normandie and increasing by as much as 0.70 % in Languedoc-Roussillon.

In Belgium, GDP continues to decline slightly in Bruxelles-Capitale (−0.25 % per year), while the strongest growth rates are projected for the northern regions and Brabant Wallon (+1.44%). Purchasing power increases by around 1.5 % in most regions, except in Bruxelles-Capitale (+1.30 %). Educational attainment improves most rapidly in Oost-Vlaanderen (+1.70 %) and least in Bruxelles-Capitale (+1.23%). Employment growth is relatively homogeneous across regions, at approximately 0.9 % per year. NO2 emissions are projected to continue rising in densely urbanized or industrial regions, notably Bruxelles, Oost-Vlaanderen, and Hainaut.

The resulting life expectancy forecasts, incorporating extrapolated economic variables, are reported in column (b) of Tables 8 and 9. For nearly all French regions, accounting for future economic developments leads to gains in life expectancy, albeit with substantial heterogeneity. The largest improvements are predicted for Ile de France (+3.11 years), Nord-Pas de Calais (+2.15 years), and Haute-Normandie (+2.14 years). In 2033, Ile de France exhibits the highest projected life expectancy (88.24 years), while Nord-Pas-de-Calais remains the lowest (83.07 years). In Belgium, the forecasts continue to display a pronounced north–south divide. In 2034, the highest and lowest life expectancies are predicted in West Vlaanderen (88.84 years) and Hainaut (82.47 years), respectively, as illustrated in Figure 9. Note that the Nord–Pas-de-Calais region and the Hainaut region, located on the French–Belgian border, appear to experience similar longevity conditions due to their geographical proximity and shared socio-economic characteristics.

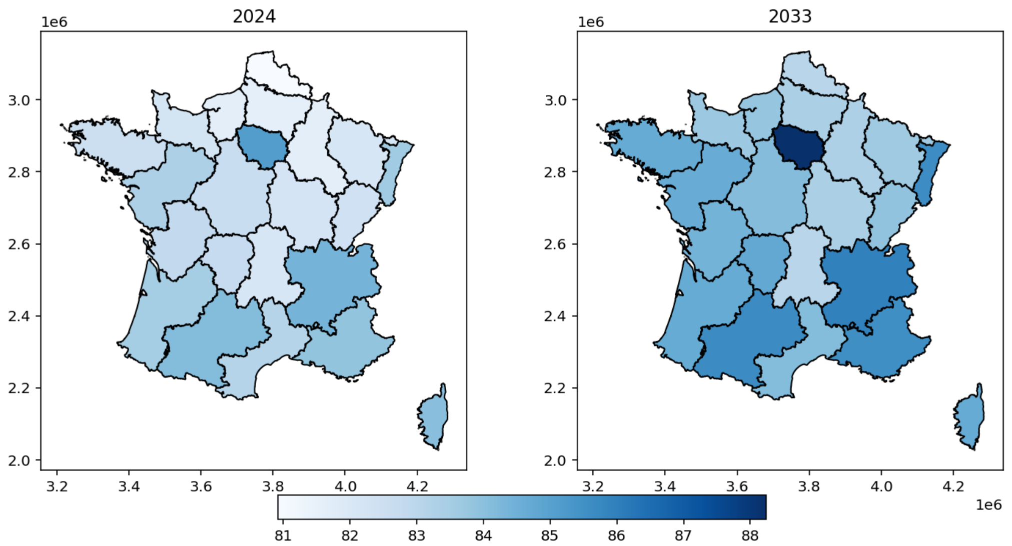

Figure 8: Comparison of NUTS 2 life expectancies in 2024 and 2033, France.

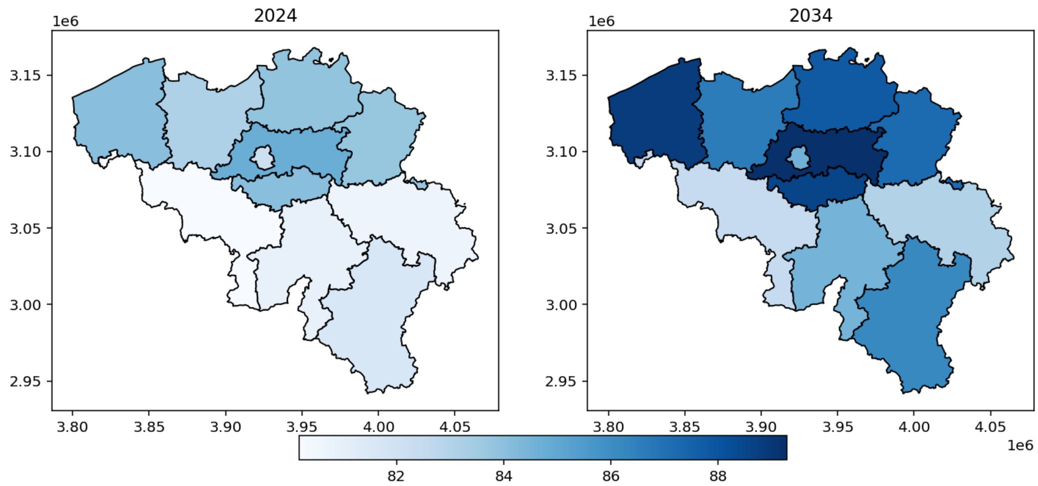

Figure 9: Comparison of NUTS 2 life expectancies in 2024 and 2033, Belgium.

Figure 8 presents the spatial distribution of French period life expectancy at birth over the period 2024–2033, as forecast by the neural network model with extrapolated economic factors. The maps clearly indicate that northern regions continue to exhibit the lowest longevity levels in France. According to our projections, this regional disparity does not narrow by 2033, suggesting a persistent north–south gradient in mortality outcomes. Conversely, no distinct geographical cluster of regions with particularly high life expectancy emerges. The three regions with the highest projected life expectancy at birth in 2033, Île-de-France (88.24 years), Rhône-Alpes (85.97 years), and Provence-Alpes-Côte d'Azur (85.56 years), are geographically dispersed and not contiguous, highlighting the absence of a clear spatial concentration of longevity advantages.

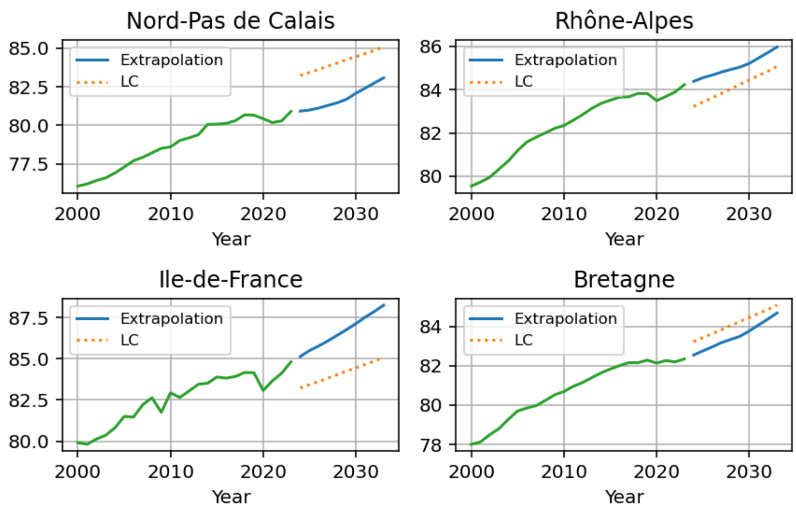

Figure 10: Evolution of life expectancies in four French regions.

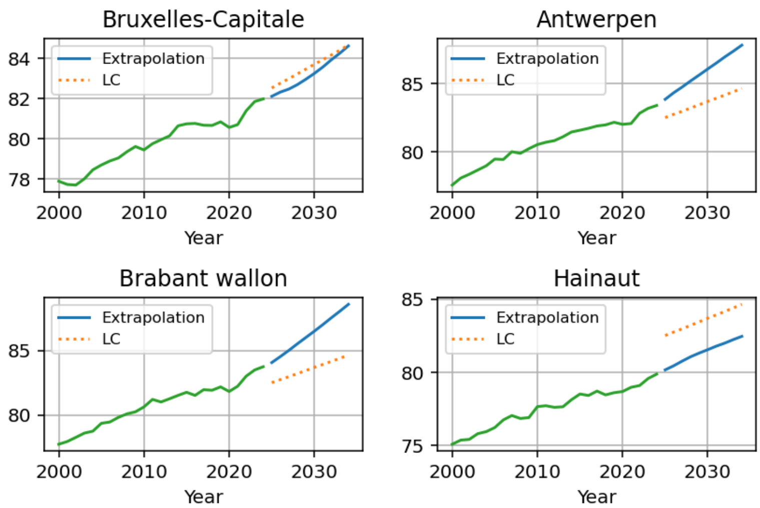

Figure 11: Evolution of life expectancies in four Belgian regions.

Figure 10 illustrates the historical and projected evolution of period life expectancy at birth in four French regions, comparing forecasts obtained with extrapolation of economic factors. The figure also reports life expectancy forecasts produced by the Lee–Carter model, for which the latent mortality index κ_t^{LC} is extrapolated using a random walk with drift.

The comparison highlights sizeable discrepancies between regional life expectancies derived from the neural network model and those implied by the national Lee–Carter framework. In Nord–Pas-de-Calais, the projected life expectancy is approximately 2 years lower than that obtained under the Lee–Carter model, whereas in Ile-de-France it exceeds the Lee–Carter forecast by nearly three years in 2033. These differences illustrate the limitations of national mortality models in capturing persistent regional heterogeneity. The implications of such discrepancies for the valuation of life annuities are examined in the next section.

Figure11 also displays the evolution of life expectancy in four Belgian regions. In this case, the Lee–Carter model systematically underestimates life expectancy at birth in Antwerpen and

Brabant Wallon.

To identify the economic factors that most strongly influence the neural network, Tables 10 and 11 in Appendix D present the changes in forecasted life expectancies for 2024 (France) and 2025 (Belgium) resulting from a marginal 10% shock applied to each economic variable. These values are computed under a single scenario using average projected economic conditions. It is important to emphasise that these figures are intended to illustrate how the neural network constructs mortality curves from economic inputs. The insights derived from the network's internal behaviour should not be interpreted as direct evidence of the true causal impact of economic factors on life expectancy.

For France, a 10% increase in GDP has only a limited effect on life expectancy, except in Île-de-France. More unexpectedly, GDP growth slightly reduces life expectancy in several regions. By contrast, a 10% rise in household purchasing power has a much more substantial impact, increasing life expectancy by roughly one year on average across all regions. Higher regional education levels also improve life expectancy, although the magnitude of the effect varies widely between areas. An increase in NO2 emissions tends to shorten life expectancy, but not uniformly across all regions.

For Belgium, a 10% increase in GDP produces a broader range of effects on life expectancy, both positive and negative depending on the region. As in France, an increase of 10% in household purchasing power raises the estimated life expectancy by about one year on average. Higher regional education levels also improve life expectancy, though only in 6 out of the 11 regions. The neural network appears particularly sensitive to the employment rate: a 10% increase can lead to gains of up to two and a half years in three Flemish regions. Finally, higher NO_2 concentrations slightly reduce life expectancy.

Nevertheless, these findings should be interpreted with caution: economic variables are correlated, and marginal shocks analyzed in isolation may lead to counter-intuitive or non-causal interpretations.

4.3 Pricing

To assess the actuarial consequences of regional mortality heterogeneity, we construct prospective life tables by extrapolating death rates up to the year 2050. Based on these projections, we price temporary life annuities with a maturity of 20 years, issued in 2023 (France) or 2024 (Belgium) to individuals aged 60 and 65. In order to isolate the effect of longevity risk and avoid confounding it with financial assumptions, the interest rate is set to zero. Mortality uncertainty is taken into account by generating 1,000 stochastic paths of future death rates, and annuity values are computed in each scenario.

Tables 12 and 13 in Appendix E, report, by region, the average annuity prices, their standard deviations, and the 5%–95% empirical percentiles. For benchmarking purposes, the same annuities are also priced using mortality scenarios generated from the Lee–Carter (LC) model.

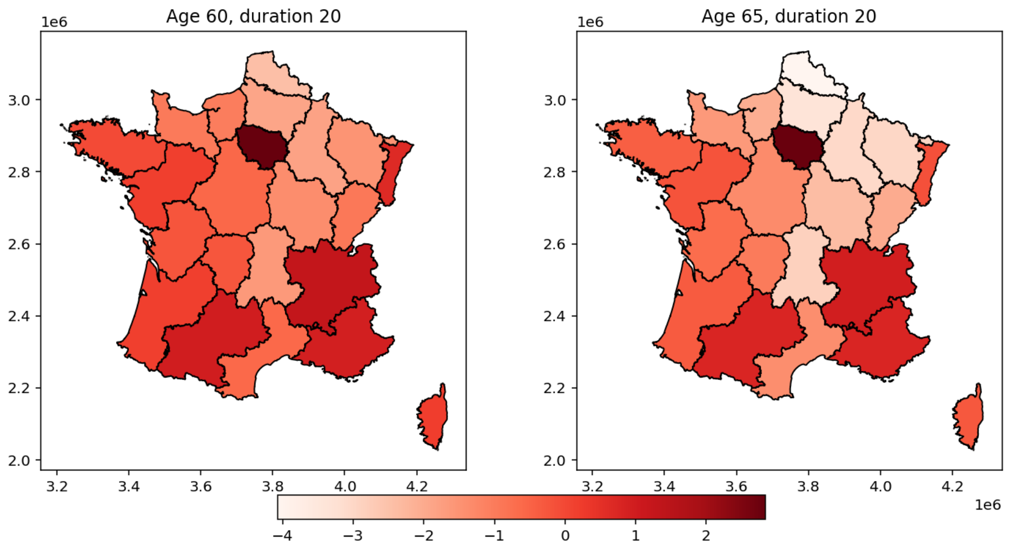

Figure 12: Map of relative spreads, between prices of a 20 years life annuity, computed with the LC and NN models. France.

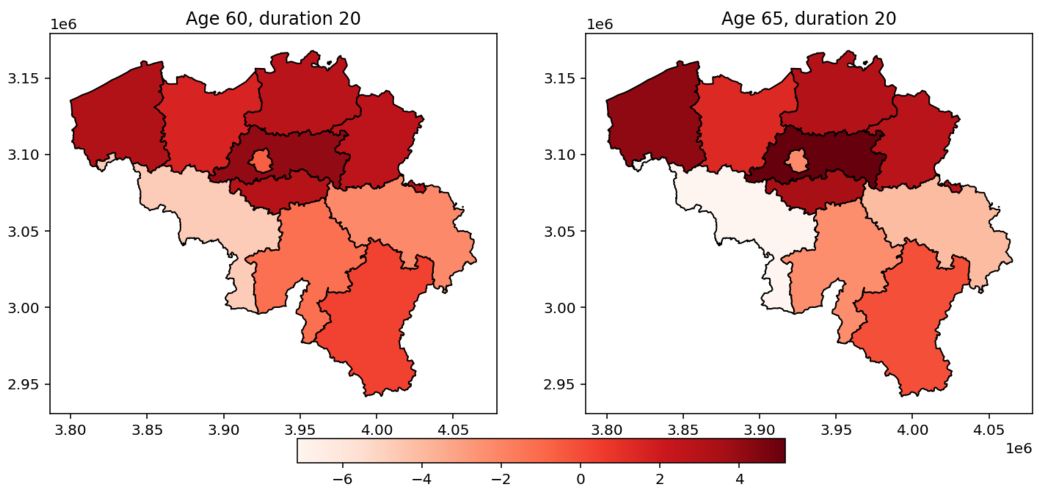

Figure 13: Map of relative spreads, between prices of a 20 years life annuity, computed with the LC and NN models. Belgium.

Figures 12 and 13 display the relative pricing spread between the neural network (NN) and LC models, defined as

$$\text{relative spread (\%)} = 100 \times \frac{\text{Average Price NN} - \text{Average Price LC}}{\text{Average Price LC}}.$$

These maps clearly show that, in most French and Belgian regions, annuities priced using the national Lee–Carter model are undervalued relative to prices obtained with the regional NN model. With the exception of a few northern French regions, reliance on the LC framework therefore leads to systematic technical losses driven by an underestimation of regional longevity improvements.

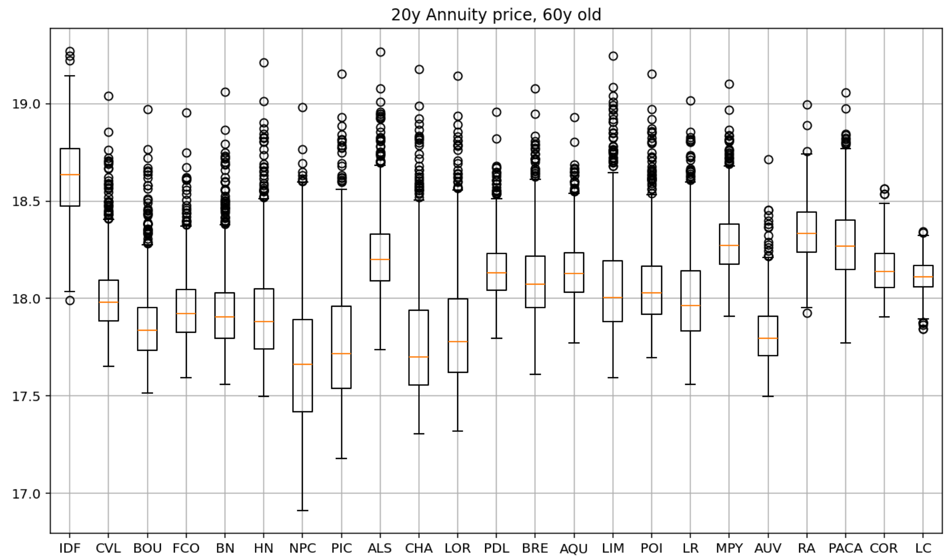

Figure 14: Boxplot of 20 y. annuity prices ($x = 60$), computed with NN and LC models, 1000 scenarios, France.

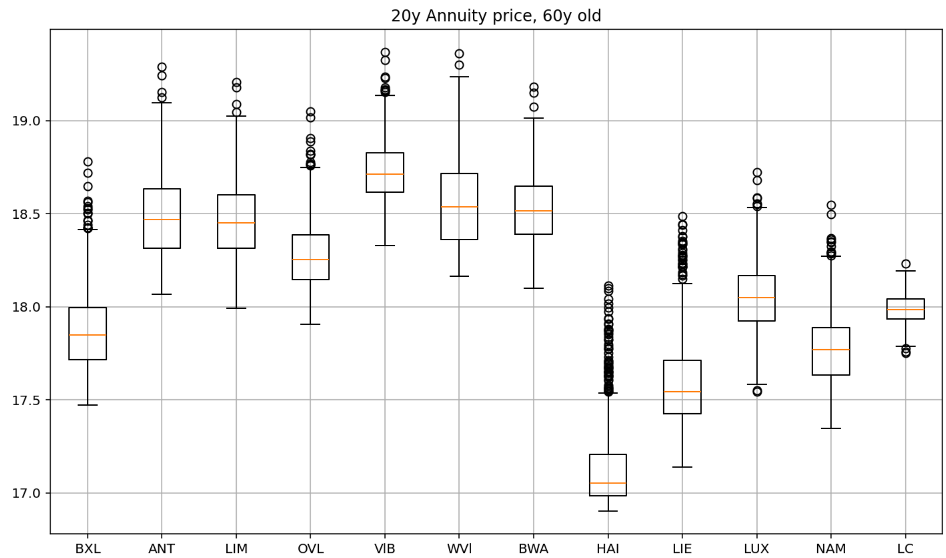

Figure 15: Boxplot of 20 y. annuity prices ($x = 60$), computed with NN and LC models, 1000 scenarios, Belgium.

Figure 14 presents boxplots of 20-year annuity prices for 60-year-old policyholders across French regions. The rightmost box corresponds to prices computed with the national Lee–Carter model. Ten regions exhibit average annuity values that are lower than the LC benchmark price (18.11). Moreover, substantial heterogeneity is observed in the dispersion of simulated prices. The highest price volatilities occur in Ile de France (0.21), while the lowest are observed in Corse (0.12), and are greater than the volatility implied by the LC model (0.08). This dispersion directly translates into region-specific differences in the solvency capital required to cover longevity risk. In particular, SCRs computed under the LC framework underestimate both the level and the variability of longevity risk in most regions.

Figure 15 shows the corresponding boxplots for Belgian regions. Average annuity prices exceed the LC benchmark (17.99) in all Flemish regions (Antwerpen, Limburg, Oost-Vlaanderen, Vlaams Brabant, and West-Vlaanderen), as well as in Brabant Wallon and Luxembourg. Price volatility is likewise higher in these regions (around 0.20) and systematically exceeds that implied by the LC model (0.08). As in the French case, the use of national Lee–Carter mortality tables for annuity pricing in Belgium would therefore result in persistent technical losses and an underestimation of the solvency capital required to manage regional longevity risk.

5 Conclusions

This article proposes an economic–neural framework for modeling and forecasting regional mortality rates, with a particular focus on actuarial applications such as life annuity pricing. By combining a feed-forward neural network with a B-spline representation of age profiles, the model addresses two major challenges inherent to regional mortality analysis: the volatility of crude death rates in small populations and the need to incorporate exogenous drivers of mortality differences across regions.

From a methodological perspective, the proposed approach offers several notable advantages. First, the use of B-splines ensures smooth and stable mortality curves across ages, a property that is essential for actuarial valuation and that is not guaranteed by fully non-parametric multi-population models. Second, the neural network structure allows mortality patterns to be linked explicitly to a set of interpretable economic variables. Unlike approaches relying on latent factors or principal components alone, this framework makes it possible to assess how changes in regional economic conditions translate into differences in mortality levels and trends. Third, empirical results for France and Belgium show that the model significantly improves the goodness of fit relative to a regional Lee–Carter specification, while avoiding the severe overfitting and irregular age profiles observed in Li–Lee–type models when applied to small regional populations. These properties make the model particularly well suited for long-term forecasting and scenario analysis.

At the same time, the approach is not without limitations. The reliance on neural networks inevitably increases model complexity and the number of parameters. Moreover, the forecasting of mortality also depends on the extrapolation of economic factors, for which the proposed SVD-based method provides robustness but remains a simplified representation of future macroeconomic dynamics. These limitations suggest that results should be interpreted with caution at a very granular level.

Despite these caveats, the actuarial implications of the results are clear and substantial. The analysis highlights persistent and economically meaningful disparities in mortality and life expectancy across regions within the same country. Ignoring these disparities by relying on national mortality tables or homogeneous projection models leads to systematic biases in the pricing of life annuities. In most regions considered, annuities priced using a national Lee–Carter model are undervalued relative to prices obtained from the regional economic–neural model, resulting in an underestimation of longevity risk and, consequently, of the solvency capital required to cover that risk. The magnitude of these pricing differences demonstrates that regional heterogeneity is not a second-order effect but a fundamental component of longevity risk.

More broadly, the findings emphasize that mortality is shaped by deeply uneven socio-economic conditions across regions, and that these differences are unlikely to vanish in the near future. For insurers and pension providers, incorporating regional mortality dynamics is therefore not only a refinement but a necessity for sound risk management, fair pricing, and adequate capital assessment. From a policy perspective, the model also provides a quantitative tool to evaluate how regional economic policies may indirectly affect longevity outcomes.

In conclusion, this work shows that combining economic information with modern machine-learning techniques and actuarially sound smoothing tools offers a promising avenue for regional mortality modeling. While further extensions are needed to refine forecasts and improve interpretability, the results already make a strong case for moving beyond national averages and explicitly accounting for regional mortality disparities when pricing life annuities and managing longevity risk.

Appendix A

This section presents the mean absolute errors between observed and predicted death rates, weighted by exposures, for NUTS2 regions of France and Belgium.

						Variation (%)	
Nuts 2	Regions	Label	Lee-Carter	NN (32,16,8)	Li & Lee	LC to NN	LC to LL
FR10	Ile-de-France	IDF	0.0002	0.0004	0.0002	-62.62	-62.46
FRB0	Centre - Val de Loire	CVL	0.0003	0.0003	0.0003	-1.55	-11.13
FRC1	Bourgogne	BOU	0.0004	0.0004	0.0004	-15.52	-17.62
FRC2	Franche-Comté	FCO	0.0004	0.0004	0.0004	-5.93	-6.7
FRD1	Basse-Normandie	BN	0.0004	0.0005	0.0004	-14.64	-15.7
FRD2	Haute-Normandie	HN	0.0003	0.0007	0.0003	-48.66	-50.63
FRE1	Nord-Pas de Calais	NPC	0.0003	0.0014	0.0003	-79.46	-79.51
FRE2	Picardie	PIC	0.0004	0.0009	0.0003	-61.99	-63.68
FRF1	Alsace	ALS	0.0003	0.0005	0.0003	-32.26	-36.78
FRF2	Champagne	CHA	0.0004	0.0007	0.0004	-41.88	-44.16
FRF3	Lorraine	LOR	0.0003	0.0007	0.0003	-54.25	-57.3
FRG0	Pays de la Loire	PDL	0.0002	0.0004	0.0002	-32.14	-36.45
FRH0	Bretagne	BRE	0.0003	0.0004	0.0003	-27.53	-28.24
FRI1	Aquitaine	AQU	0.0003	0.0004	0.0003	-32.75	-35.1
FRI2	Limousin	LIM	0.0006	0.0006	0.0005	-0.26	-5.91
FRI3	Poitou-Charentes	POI	0.0004	0.0005	0.0003	-23.78	-25.74
FRJ1	Languedoc-Roussillon	LR	0.0003	0.0004	0.0003	-25.27	-26.85
FRJ2	Midi-Pyrénées	MPY	0.0003	0.0006	0.0002	-55.0	-58.59
FRK1	Auvergne	AUV	0.0004	0.0005	0.0004	-14.57	-19.87
FRK2	Rhône-Alpes	RA	0.0002	0.0005	0.0002	-61.82	-62.73
FRL0	Provence-Alpes-Côte d'Azur	PACA	0.0002	0.0004	0.0002	-43.28	-45.96
FRM0	Corse	COR	0.0008	0.0009	0.0008	-10.16	-11.89
	Global		0.0003	0.0005	0.0003	-49.44	-51.22

Table 4: Table of weighted mean absolute errors (WMAE), France.

Nuts 2	Regions	Label	Lee-Carter	NN (32,16,8)	Li & Lee	Variation (%) LC to NN	LC to LL
BE10	Bruxelles	BXL	0.0004	0.0005	0.0004	-21.04	-16.3
BE21	Antwerpen	ANT	0.0003	0.0006	0.0003	-43.96	-44.61
BE22	Limburg	LIM	0.0004	0.0008	0.0004	-44.92	-44.22
BE23	Oost-Vlaanderen	OVL	0.0004	0.0005	0.0004	-21.99	-25.71
BE24	Vlaams Brabant	VlB	0.0004	0.0008	0.0004	-51.58	-52.04
BE25	West-Vlaanderen	WVl	0.0004	0.0008	0.0004	-50.35	-52.28
BE31	Brabant wallon	BWA	0.0007	0.0008	0.0007	-13.79	-16.06
BE32	Hainaut	HAI	0.0005	0.0015	0.0005	-67.6	-69.27
BE33	Liège	LIE	0.0005	0.001	0.0005	-50.37	-52.62
BE34	Luxembourg	LUX	0.0009	0.001	0.0009	-15.84	-16.59
BE35	Namur	NAM	0.0007	0.0011	0.0007	-36.28	-37.7
	Global		0.0004	0.0008	0.0004	-45.83	-46.9

Table 5: Table of weighted mean absolute errors (WMAE), Belgium.

Appendix B

In Sub-Section 4.2, we extrapolate economic variables up to 2033 (FR) and 2034 (BE) using a 2 dimensions reduction. Tables 6 and 7, report the average growth rates of simulated economic factors for French and Belgian NUTS2 regions.

Nuts 2	Label	Yearly average growth rates (%) GDP	PPS	EDU	EMP	NO2
FR10	IDF	1.72	1.40	1.47	0.97	0.11
FRB0	CVL	1.42	1.33	1.63	0.89	0.44
FRC1	BOU	1.45	1.36	1.70	1.00	0.41
FRC2	FCO	1.31	1.38	1.66	0.93	0.43
FRD1	BN	1.39	1.44	1.52	0.92	0.42
FRD2	HN	1.44	1.36	1.66	0.90	-1.16
FRE1	NPC	1.55	1.43	1.75	0.99	-0.07
FRE2	PIC	1.40	1.31	1.67	0.89	0.16
FRF1	ALS	1.51	1.33	1.42	0.90	-1.05
FRF2	CHA	1.29	1.32	1.59	0.78	0.44
FRF3	LOR	1.29	1.37	1.63	0.89	0.31
FRG0	PDL	1.72	1.43	1.66	1.01	0.36
FRH0	BRE	1.65	1.44	1.56	1.01	0.42
FRI1	AQU	1.69	1.41	1.65	1.06	0.07
FRI2	LIM	1.42	1.35	1.62	0.94	0.34
FRI3	POI	1.60	1.37	1.65	0.96	0.44
FRJ1	LR	1.66	1.39	1.61	1.09	0.70
FRJ2	MPY	1.79	1.43	1.57	0.97	0.42
FRK1	AUV	1.57	1.41	1.51	1.00	0.38
FRK2	RA	1.68	1.44	1.64	1.03	0.36
FRL0	PACA	1.73	1.44	1.70	1.14	0.59
FRM0	COR	1.85	1.60	2.27	1.60	0.35

Table 6: Average yearly growth rates in % of simulated economic factors between 2023 and 2033, France.

Nuts 2	Label	Yearly average growth rates (%) GDP	PPS	EDU	EMP	NO2
BE10	BXL	-0.25	1.3	1.23	0.89	0.75
BE21	ANT	0.66	1.48	1.54	1.01	0.08
BE22	LIM	0.59	1.57	1.68	1.07	0.16
BE23	OVL	0.86	1.56	1.7	1.02	0.58
BE24	VlB	0.84	1.46	1.46	0.85	0.25
BE25	WVl	0.86	1.6	1.65	0.99	0.35
BE31	BWA	1.44	1.48	1.42	0.95	0.23
BE32	HAI	0.46	1.56	1.54	0.86	0.85
BE33	LIE	0.71	1.55	1.55	0.84	0.39
BE34	LUX	0.25	1.63	1.63	0.87	0.05
BE35	NAM	0.57	1.6	1.6	0.91	0.22

Table 7: Average yearly growth rates in % of simulated economic factors between 2024 and 2034, Belgium.

Appendix C

This section presents life expectancy forecasts with and without extrapolation of economic factors for France and Belgium, over 10 years.

Nuts 2	Label	2024 (a) projected factors	2033 (b) projected factors	(b) - (a)
FR10	IDF	85.13	88.24	3.11
FRB0	CVL	82.64	84.1	1.46
FRC1	BOU	82.22	83.37	1.15
FRC2	FCO	82.42	83.92	1.5
FRD1	BN	82.26	83.71	1.45
FRD2	HN	81.69	83.83	2.14
FRE1	NPC	80.92	83.07	2.15
FRE2	PIC	81.61	83.36	1.75
FRF1	ALS	83.59	85.61	2.02
FRF2	CHA	81.66	83.34	1.68
FRF3	LOR	82.13	83.66	1.53
FRG0	PDL	83.34	84.64	1.3
FRH0	BRE	82.54	84.67	2.13
FRI1	AQU	83.51	84.68	1.17
FRI2	LIM	82.76	84.77	2.01
FRI3	POI	82.86	84.43	1.57
FRJ1	LR	83.13	84.13	1.0
FRJ2	MPY	84.14	85.64	1.5
FRK1	AUV	82.12	83.09	0.97
FRK2	RA	84.38	85.97	1.59
FRL0	PACA	83.87	85.56	1.69
FRM0	COR	84.06	84.68	0.62
LC		83.22	85.07	

Table 8: Life expectancy at birth, in years, France.

Nuts 2	Label	2025 (a) projected factors	2034 (b) projected factors	(b) - (a)
BE10	BXL	82.00	84.62	2.62
BE21	ANT	83.5	87.82	4.32
BE22	LIM	83.69	87.26	3.57
BE23	OVL	83.02	86.64	3.62
BE24	VlB	84.31	89.29	4.98
BE25	WVl	83.76	88.84	5.08
BE31	BWA	83.75	88.59	4.84
BE32	HAI	80.16	82.47	2.31
BE33	LIE	80.84	83.05	2.21
BE34	LUX	81.53	86.16	4.63
BE35	NAM	80.94	84.5	3.56
LC		82.53	84.66	

Table 9: Life expectancy at birth, in years, Belgium.

Appendix D

This section reports the changes in forecasted life expectancies, in 2024 (FR) and 2025 (BE), after a marginal shock of 10% in economic factors.

Nuts 2	Label	2024	GDP	PPS	EDU	EMP	NO2
FR10	IDF	85.09	3.05	1.82	0.73	0.12	0.67
FRB0	CVL	82.54	-0.04	0.8	0.52	0.18	-0.17
FRC1	BOU	82.19	-0.05	0.83	0.17	-0.08	-0.17
FRC2	FCO	82.31	-0.03	1.0	0.51	1.0	-0.12
FRD1	BN	82.2	-0.05	0.95	0.36	0.0	-0.22
FRD2	HN	81.57	-0.10	1.75	0.23	-0.3	0.2
FRE1	NPC	80.9	-0.12	1.46	1.07	-1.79	0.31
FRE2	PIC	81.59	-0.14	1.59	0.26	-1.41	-0.02
FRF1	ALS	83.51	-0.09	1.59	0.86	0.11	-0.14
FRF2	CHA	81.64	-0.08	1.55	0.23	-0.58	-0.2
FRF3	LOR	82.1	-0.11	1.6	0.21	-0.84	-0.11
FRG0	PDL	83.33	-0.04	0.51	0.51	0.19	-0.18
FRH0	BRE	82.36	0.03	1.45	1.43	0.19	-0.12
FRI1	AQU	83.48	-0.13	0.76	0.61	0.02	-0.14
FRI2	LIM	82.71	-0.04	1.0	0.81	-0.49	-0.1
FRI3	POI	82.8	-0.06	1.06	0.21	-0.23	-0.26
FRJ1	LR	82.97	-0.10	1.57	1.15	-0.82	-0.11
FRJ2	MPY	84.12	-0.11	0.83	0.83	0.19	-0.15
FRK1	AUV	82.07	-0.04	0.73	0.26	0.5	-0.13
FRK2	RA	84.35	0.11	0.88	1.23	-0.08	-0.03
FRL0	PACA	83.78	0.03	1.42	1.33	-0.39	-0.04
FRM0	COR	84.01	-0.01	1.18	0.17	-0.74	-0.03

Table 10: Impact of a 10% shift of economic factors on regional life expectancies in 2024, France.

Nuts 2	Label	2025	GDP	PPS	EDU	EMP	NO2
BE10	BXL	82.11	1.07	1.12	0.27	0.72	-0.42
BE21	ANT	83.78	0.22	0.61	0.04	2.5	-0.19
BE22	LIM	83.68	-0.35	0.43	0.04	1.27	-0.13
BE23	OVL	83.12	-0.58	0.73	-0.64	2.83	-0.34
BE24	VlB	84.56	0.1	1.53	0.55	2.52	-0.19
BE25	WVl	83.92	0.17	0.94	-0.28	2.46	-0.06
BE31	BWA	84.07	0.41	1.32	0.6	1.72	-0.21
BE32	HAI	80.13	-1.0	1.15	-1.0	0.56	0.4
BE33	LIE	80.62	-0.69	0.51	-0.54	0.21	-0.12
BE34	LUX	81.47	-0.54	1.13	0.5	0.19	-0.04
BE35	NAM	80.77	-0.53	0.8	-0.19	0.5	-0.12

Table 11: Impact of a 10% shift of economic factors on regional life expectancies, in 2025, Belgium.

Appendix E

This section reports the average prices, the standard deviations (Std) and 5% - 95% percentiles of two life annuities, by French and Belgian regions. We consider 20 years temporary life annuities purchased in 2023 (FR) and 2024 (BE) by 60 and 65 years old customers.

		20 y. , $x = 60$				20 y. , $x = 65$			
Nuts 2	Label	Price	Std	5%	95%	Price	Std	5%	95%
FR10	IDF	18.62	0.21	18.27	18.97	17.83	0.27	17.4	18.27
FRB0	CVL	18.01	0.19	17.76	18.35	17.12	0.24	16.78	17.55
FRC1	BOU	17.87	0.2	17.61	18.22	16.93	0.25	16.61	17.38
FRC2	FCO	17.94	0.17	17.7	18.23	17.0	0.23	16.67	17.39
FRD1	BN	17.94	0.21	17.67	18.34	17.07	0.27	16.71	17.57
FRD2	HN	17.93	0.25	17.6	18.41	16.99	0.31	16.6	17.57
FRE1	NPC	17.67	0.34	17.14	18.23	16.64	0.4	16.03	17.33
FRE2	PIC	17.77	0.32	17.35	18.38	16.77	0.4	16.26	17.55
FRF1	ALS	18.23	0.21	17.94	18.61	17.32	0.27	16.95	17.82
FRF2	CHA	17.78	0.31	17.43	18.41	16.82	0.39	16.38	17.62
FRF3	LOR	17.84	0.29	17.46	18.41	16.83	0.38	16.35	17.57
FRG0	PDL	18.14	0.15	17.91	18.42	17.32	0.2	17.02	17.64
FRH0	BRE	18.1	0.22	17.79	18.5	17.28	0.27	16.89	17.78
FRI1	AQU	18.14	0.16	17.9	18.43	17.29	0.21	16.96	17.66
FRI2	LIM	18.06	0.26	17.73	18.6	17.18	0.34	16.74	17.84
FRI3	POI	18.07	0.22	17.8	18.49	17.23	0.27	16.88	17.75
FRJ1	LR	18.0	0.24	17.69	18.46	17.11	0.3	16.71	17.68
FRJ2	MPY	18.29	0.17	18.03	18.59	17.48	0.22	17.14	17.88
FRK1	AUV	17.81	0.15	17.59	18.05	16.85	0.2	16.56	17.19
FRK2	RA	18.34	0.15	18.11	18.59	17.52	0.19	17.21	17.83
FRL0	PACA	18.28	0.19	17.99	18.62	17.48	0.25	17.11	17.91
FRM0	COR	18.15	0.12	17.96	18.36	17.3	0.17	17.06	17.59
LC		18.11	0.08	17.97	18.24	17.35	0.14	17.11	17.56

Table 12: Statistics about prices of 20 years temporary life annuities, by French region.

		20 y. , $x=60$				20 y. , $x=65$			
Nuts 2	Label	Price	Std	5%	95%	Price	Std	5%	95%
BE10	BXL	17.87	0.21	17.58	18.25	16.65	0.27	16.29	17.14
BE21	ANT	18.49	0.21	18.18	18.85	17.55	0.29	17.15	18.06
BE22	LIM	18.47	0.2	18.16	18.81	17.51	0.27	17.12	17.98
BE23	OVL	18.28	0.18	18.04	18.59	17.26	0.2	16.99	17.63
BE24	VlB	18.73	0.15	18.5	19.0	17.91	0.21	17.6	18.28
BE25	WVl	18.56	0.23	18.23	18.94	17.74	0.3	17.33	18.27
BE31	BWA	18.53	0.18	18.26	18.85	17.62	0.23	17.29	18.04
BE32	HAI	17.13	0.21	16.94	17.57	15.81	0.3	15.54	16.44
BE33	LIE	17.59	0.24	17.28	18.05	16.33	0.3	15.95	16.92
BE34	LUX	18.05	0.18	17.76	18.34	17.01	0.22	16.66	17.38
BE35	NAM	17.78	0.19	17.5	18.11	16.63	0.24	16.29	17.04
LC		17.99	0.08	17.87	18.11	17.03	0.12	16.83	17.23

Table 13: Statistics about prices of 20 years temporary life annuities, by Belgian region.

Acknowledgment

I thank the FNRS (Fonds de la recherche scientifique) for the financial support through the EOS project Asterisk (research grant 40007517).

Statements and declarations

The author has seen and agree with the contents of the manuscript and there is no financial interest to report.

References

[1] Cairns A.J.G., Blake D., Dowd K. 2008. Modelling and management of mortality risk: a review. Scandinavian Actuarial Journal, 2008 (2–3), 79-113

[2] Boonen T.J., Li H. 2017. Modeling and forecasting mortality with economic growth: a multipopulation approach. Demography 54(5), 1921–1946.

[3] Booth H., Tickle L. 2011. Mortality modelling and forecasting: a review of methods. Annals of Actuarial Sciences 3(1-2), 3-43.

[4] Brenner M.H. 2005. Commentary: economic growth is the basis of mortality rate decline in the 20th century experience of the United States 1901–2000. International Journal of Epidemiology, 34(6), 1214–1221.

[5] Brouhns N., Denuit M., Vermunt J. 2002. A Poisson log-bilinear regression approach to the construction of projected lifetables. Insurance: Mathematics and Economics, 31(3), 373-393.

[6] Birchenall J.A. 2007. Economic development and the escape from high mortality. World Development. 35(4), 543–568.

[7] Carmarda C.G. 2019. Smooth constrained mortality forecasting. Demographic research 41, 1091-1130.

[8] Denuit M., Hainaut. D., Trufin J., 2019. Effective Statistical Learning Methods for Actuaries III. Neural Networks and Extensions. Springer actuarial Lectures Notes. Springer Nature Switzerland AG.

[9] Dimai M. 2024. Modeling and forecasting mortality with economic, environmental and lifestyle variables. Decisions in Economics and Finance https://doi.org/10.1007/s10203-024-00434-4

[10] French D., O'Hare C. 2014. Forecasting death rates using exogenous determinants. Journal of Forecasting, 33, 640–650.

[11] Hainaut D. 2018. A neural network analyzer for mortality forecast. ASTIN Bulletin 48(2), 481-508.

[12] Hainaut D. 2026. An economic-environmental approach for regional mortality. ISBA-UCLouvain, discussion paper.

[13] Hyndman R. J., Booth H., Yasmeen F., 2013. Coherent mortality forecasting: The product-ratio method with functional time series models. Demography, 50, 261–283.

[14] Li N., Lee R.D., 2005. Coherent mortality forecasts for a group of populations: An extension of the Lee-Carter method. Demography 57, 575-594.

[15] Lee R. D., Carter L. R., 1992. Modeling and forecasting U.S. mortality. Journal of the American Statistical Association, 87, 659–671.

[16] Niu G., Melenberg B., 2014. Trends in mortality decrease and economic growth. Demography, 51(5), 1755–1773.

[17] Oirov T., Terbish G., Dorj N. 2021. B-spline Estimation for Force of Mortality. Mathematics and Statistics, 9(5), 736-743

[18] Pavone F., Legramanti S., Durante D. 2024. Learning and forecasting of age-specific period mortality via B-spline processes with locally-adaptive dynamic coefficients. The Annals of Applied Statistics 18 (3), 1965-1987.

[19] Plat R., 2009. On stochastic mortality modeling. Insurance: Mathematics and Economics, 45(3), 393-404.

[20] Renshaw A.E., Haberman S., 2006. A cohort-based extension to the Lee-Carter model for mortality reduction factors. Insurance: Mathematics and Economics, 38(3), 556–570

[21] Ruhm C.J., 2005. Commentary: Mortality increases during economic upturns. International Journal of Epidemiology, 34, 1206-1211.

[22] Tapia Granados J. A., Roux A.V.D. 2009. Life and death during the Great Depression. Proceedings of the National Academy of Sciences, 106, 17290–17295.

[23] Villegas A.M., Bajekal M., Haberman S. 2025. Modelling mortality by cause of death and socio-economic stratification: an analysis of mortality differentials in England. Decisions in Economics and Finance. https://doi.org/10.1007/s10203-025-00511-2